

FastVGGT: Training-Free Acceleration of Visual Geometry Transformer

You Shen¹, Zhipeng Zhang², Yansong Qu¹, Liujuan Cao^{1*}

¹Key Laboratory of Multimedia Trusted Perception and Efficient Computing,
Ministry of Education of China, Xiamen University

²AutoLab, School of Artificial Intelligence, Shanghai Jiao Tong University

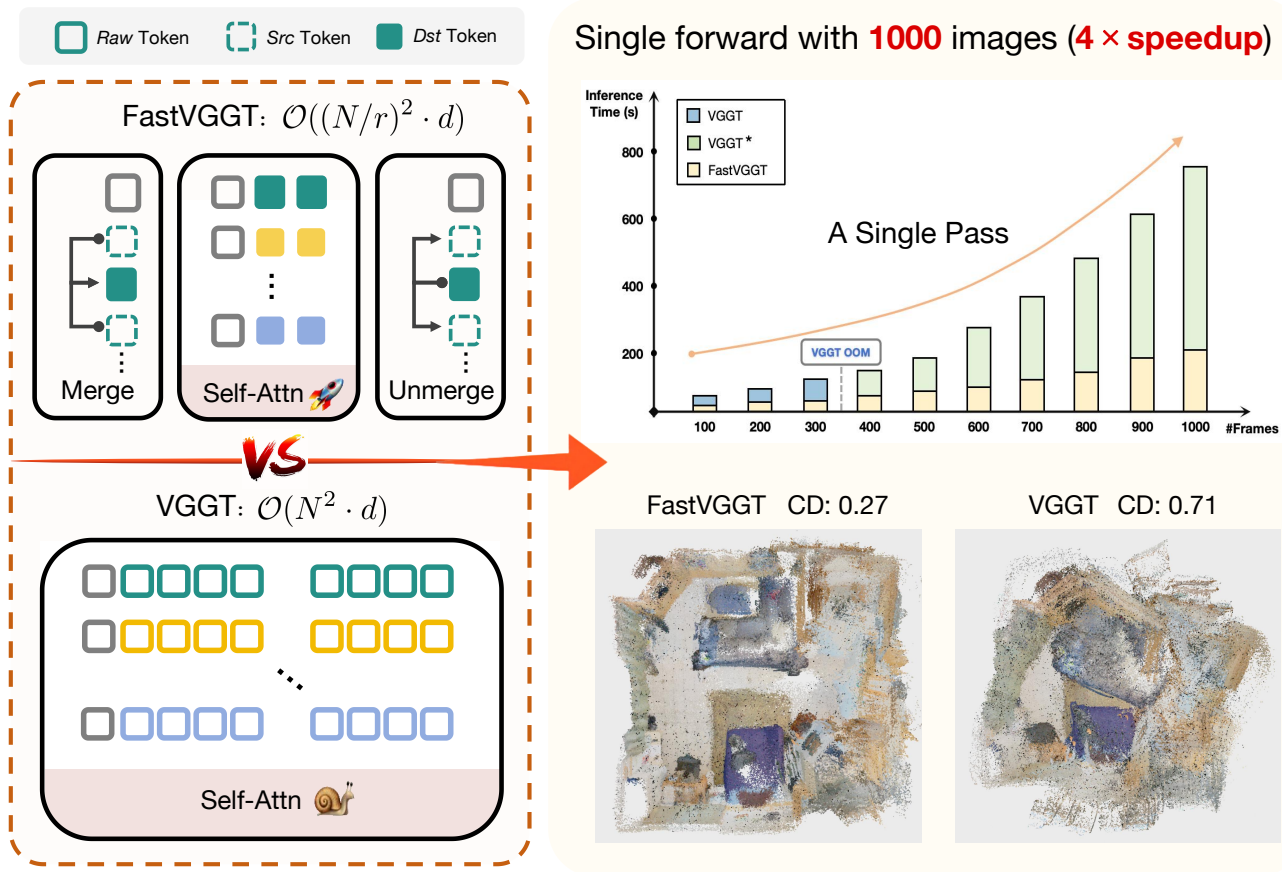


Figure 1. In contrast to VGGT, which performs dense interactions across all scene tokens, FastVGGT adopts token merging to restrict interactions to a compact subset. For 1000 input images, it achieves more than a 4× speedup in inference with reduced error accumulation. VGGT* refers to VRAM-Efficient of VGGT, enabling larger inputs.

Abstract

Foundation models for 3D vision have recently demonstrated remarkable capabilities in 3D perception. However, scaling these models to long-sequence image inputs remains a significant challenge due to inference-time in-

efficiency. In this work, we present a detailed analysis of VGGT, a state-of-the-art feed-forward visual geometry model and identify its primary bottleneck. Visualization further reveals a token collapse phenomenon in the attention maps. Motivated by these findings, we explore the potential of token merging in the feed-forward visual geometry model. Owing to the unique architectural and task-specific

*Corresponding Author.

properties of 3D models, directly applying existing merging techniques proves challenging. To this end, we propose *FastVGGT*, which, for the first time, leverages token merging in the 3D domain through a training-free mechanism for accelerating VGGT. we devise a unique token partitioning strategy tailored to 3D architectures and tasks, effectively eliminating redundant computation while preserving VGGT’s powerful reconstruction capacity. Extensive experiments on multiple 3D geometry benchmarks validate the effectiveness of our approach. Notably, with 1000 input images, *FastVGGT* achieves a 4× speedup over VGGT while mitigating error accumulation in long-sequence scenarios. These findings underscore the potential of token merging as a principled solution for scalable 3D vision systems. Code is available at: <https://mystorm16.github.io/fastvggt/>.

1. Introduction

Inferring the 3D geometric structure of a scene from visual inputs, is critical for enabling machines to understand and interact with the physical world. Recent advances in deep learning have catalyzed a paradigm shift in 3D geometric estimation [15, 16, 25, 27, 32], enabling a move from iterative, optimization-based pipelines to end-to-end neural networks that directly infer geometry from raw visual inputs. This transformation is exemplified by large-scale architectures like DUST3R [27] and its follow-ups [11, 23, 30], which showcase a remarkable capacity to reason about complex geometric relationships across image pairs.

Building upon this line of research, VGGT [25] marks a significant advance. Its transformer-based, feed-forward architecture directly regresses key 3D attributes, including camera parameters, depth maps, and point tracks, to achieve highly stable and accurate reconstructions. While this establishes VGGT as a state-of-the-art framework for 3D scene understanding, its scalability is impeded by two critical bottlenecks. First, the model’s reliance on dense global token interactions across views or frames results in prohibitive computational costs. Although used techniques like Flash-Attention mitigate the memory complexity from $O(n^2)$ to $O(nd)$, the underlying time complexity remains quadratic at $O(n^2d)$. Second, the global attention mechanism, essential for capturing inter-frame relations, is susceptible to error accumulation. As the token space expands with each new frame, minor inaccuracies are amplified, leading to significant prediction drift. Collectively, these limitations restrict VGGT’s applicability in large-scale scenarios and motivate the development of more efficient and scalable architectures.

To pinpoint the primary inference bottlenecks in VGGT, we first conducted a detailed, component-wise performance analysis, as illustrated in Figure 2. The analysis reveals that while the computational costs of “Frame Attention” (intra-

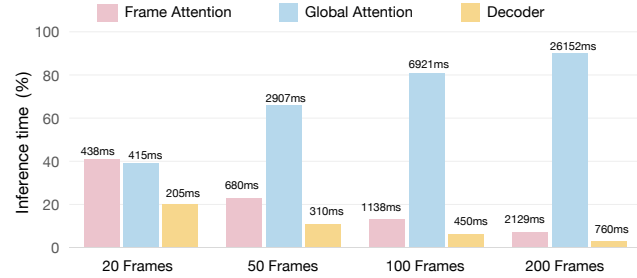


Figure 2. Component-wise analysis of VGGT inference time. As the number of input frames grows, the Global Attention module increasingly dominates the computational cost.

frame interaction) and “Global Attention” (inter-frame interaction) are comparable for short sequences, the cost of Global Attention escalates rapidly with sequence length, eventually dominating the entire runtime profile. This finding motivates our central research question: *Can the computational inefficiency of Global Attention be mitigated without compromising VGGT’s capability?* To investigate this possibility, we visualized the attention maps in Figure. 3, which uncovered a crucial insight that attention patterns across tokens exhibit a high degree of similarity, indicating substantial redundancy in the global computation.

Motivated by the observation of attention redundancy, we adapt the training-free technique of token merging [1, 2, 10, 24] to enhance VGGT’s inference efficiency. Token merging consolidates redundant representations by partitioning tokens into source (src) and destination (dst) sets and merging each src token into its most similar dst counterpart. While effective in 2D vision tasks, its extension to structures designed for 3D geometry understanding remains underexplored. Unlike 2D settings that process single images, VGGT relies on cross-image correspondences, making direct application of token merging highly challenging. To address this, we introduce *FastVGGT*, a novel, training-free framework that strategically applies token merging to mitigate the Global Attention bottleneck. Our approach begins by preserving the foundational coordinate system. Specifically, tokens from the initial frame, which serves as the global reference for the entire scene, are designated as high-priority destination (dst) tokens and are exempt from being merged to ensure reconstruction stability. Furthermore, to maintain global consistency and preserve fine-grained details, we identify and retain the most salient tokens across all frames, allowing them to bypass the merging process entirely and participate directly in the attention computation. Finally, drawing inspiration from ToMeSD [1], we implement region-based random sampling within each subsequent frame. This ensures a spatially balanced selection of src and dst tokens, preventing critical information loss in localized regions during consolidation.

Our experiments demonstrate that this integrated approach allows FastVGGT to significantly reduce the computational overhead of Global Attention. For large-scale inputs of 1000 images, it achieves $4\times$ inference speedup over the baseline VGGT while simultaneously mitigating error accumulation in long-sequence reconstructions. Notably, the original VGGT suffers from prohibitive memory consumption, leading to Out-of-Memory (OOM) errors when processing sequences beyond 300 images. Through VRAM optimization, our modified VGGT successfully handles inputs of over 1000 images, demonstrating a substantial improvement in scalability.

In summary, our main contributions are as follows: 1) We identify and analyze the key bottleneck that limits the inference speed of VGGT. 2) Based on our observation of VGGT’s Global Attention, we introduce token merging into feed-forward visual geometry architectures for the first time. 3) Extensive experiments demonstrate that our method significantly accelerates VGGT on large-scale inputs while preserving reconstruction quality and mitigating error accumulation.

2. Related work

2.1. Feed-Forward 3D Reconstruction

Building on the foundations of traditional 3D reconstruction [12, 13, 19, 21, 28], recent end-to-end learning-based methods leverage neural networks to encode scene priors, substantially enhancing robustness and cross-dataset generalization. Early progress was marked by DUSt3R [27], which directly regresses view-consistent 3D point maps from only two RGB images without requiring camera calibration. Its successor, MASt3R [11], introduces confidence-weighted losses to approximate metric scale, further improving reconstruction quality. The current state-of-the-art, VGGT [25] scales this philosophy to a 1.2B-parameter transformer that jointly predicts camera intrinsics, extrinsics, dense depth, point maps, and 2D tracks. However, as input sequences grow longer, the global attention mechanism must capture inter-frame relations within an expanding token space. This not only increases computational overhead but also amplifies noise propagation, making long-sequence predictions more prone to drift. VGGT-Long [7] addresses the drifting issue by aligning sub-maps to suppress error accumulation, but at the cost of significantly reduced inference speed, undermining the efficiency of feed-forward 3D reconstruction. To overcome these challenges, we propose FastVGGT, which accelerates inference and mitigates error accumulation by reducing the number of tokens processed in Global Attention, thereby achieving a balance between efficiency and accuracy.

2.2. Token Merging

Visual token merging [2, 9, 17, 31] was first introduced as a training-free approach to improve the throughput of Vision Transformers (ViTs) [8]. It was later extended to reduce computational cost in tasks such as diffusion, video and language understanding, and video editing [3, 5, 20]. The method partitions tokens into two sets, matches each token with its most similar counterpart, merges them via average pooling, and concatenates the results. Although simple and effective, most applications remain limited to the image domain, while long-form video remains underexplored despite its spatiotemporal tokens being both redundant and interdependent. In parallel, other approaches to token reduction have emerged. TokenLearner [18] adaptively selects informative tokens with an MLP. PuMer [3] integrates pruning and merging for vision-language models. Pooling-based methods accelerate attention by averaging token embeddings. While sharing the goal of efficient transformers, our work targets the unique demands of feed-forward 3D reconstruction, where tokens must retain spatial precision and temporal coherence. To this end, we propose FastVGGT, which adapts token merging to VGGT, achieving substantial acceleration while maintaining reconstruction fidelity.

3. Method

3.1. Visualization Findings

We highlight an observation that motivates our optimization of the Global Attention module. As shown in Figure 3, we visualize VGGT’s Global Attention maps on the ScanNet dataset. Each image is represented by 1,041 tokens (one camera token, four register tokens, and 1,036 patch tokens from a 28×37 grid). The dense self-attention mechanism generates an attention map for every token, and visualizations across tokens and blocks reveal that many of these maps are highly similar.

The phenomenon of attention similarity, often referred to as feature degradation, has been consistently reported in the DINO series [4, 14, 22]. In DINO, while the CLS token becomes increasingly discriminative, patch-level features gradually lose local consistency as they converge toward the CLS token, which undermines performance on dense prediction tasks. A similar limitation appears in VGGT: its global self-attention layers aggregate information across all tokens via weighted averaging, and without explicit regularization or task-specific constraints, the representational space is repeatedly compressed. This compression drives tokens to collapse along a dominant direction, eroding their distinctiveness. At a fundamental level, both DINO and VGGT lack explicit mechanisms to preserve token diversity, leading to a progressive loss of local variation.

It is important to note that the consequences of feature degradation differ markedly between DINO and VGGT. In

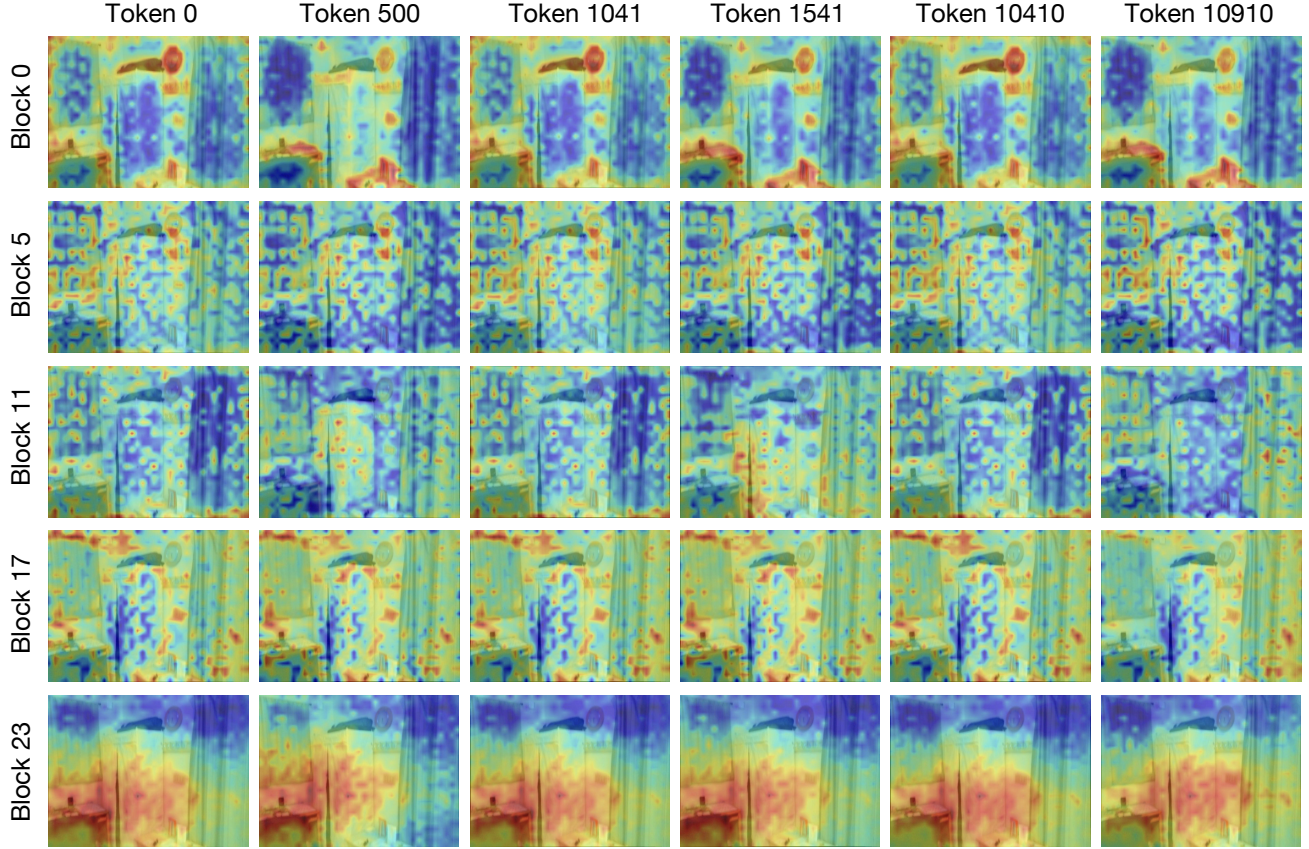


Figure 3. Visualizations of the Global Attention maps in VGGT, using six representative tokens (including the camera token and several image tokens), show that at every stage the attention patterns of different tokens exhibit a strong degree of similarity.

DINO, the network must handle not only image classification but also dense prediction tasks such as segmentation, where local feature integrity is critical. As training progresses, patch tokens collapse toward the CLS token, weakening dense feature discrimination and directly impairing downstream performance. This motivates corrective strategies such as Gram Anchoring [22]. By contrast, VGGT follows a two-stage design: Global Attention and Frame Attention. Global Attention enforces global consistency by capturing holistic spatial-temporal relationships. Here, the apparent degradation—tokens collapsing toward a dominant subspace—can be interpreted not as a flaw but as deliberate distillation of global semantics. Frame Attention then reintroduces local variability, striking a balance between global abstraction and local differentiation. Moreover, the strong feature similarity observed in Global Attention exposes redundancy that can be exploited to reduce computational cost without compromising performance, providing a natural path to address VGGT’s speed bottleneck.

Motivated by the strong similarities observed in Global Attention maps, we propose FastVGGT, which accelerates inference via token merging. Conventional strategies

	Random		Fixed		Baseline
	$r = 0.5$	$r = 0.8$	$s = 5$	$s = 8$	
CD \downarrow	0.32	0.44	0.33	0.77	0.21
Time \downarrow	22.6	16.9	17.2	11.6	30.4

Table 1. Results of applying merging strategies based on random sampling and fixed-stride sampling. Here, r denotes the merging ratio, and s represents the stride for selecting dst tokens.

typically partition tokens into destination (dst) and source (src) sets through random or fixed-stride sampling. However, the structural and task-specific requirements of 3D reconstruction make their direct application to VGGT non-trivial. To assess their suitability, we tested both random sampling (with two merging ratios) and fixed-stride sampling (with two stride settings) in VGGT’s Global Attention layer. As shown in Table 1, these methods reduce inference time but significantly increase the Chamfer Distance, thereby degrading reconstruction accuracy and failing to retain VGGT’s strong performance. To overcome this, we design a tailored strategy for feed-forward 3D reconstruction that preserves accuracy, accelerates inference, and mitigates error accumulation in long-sequence scenarios.

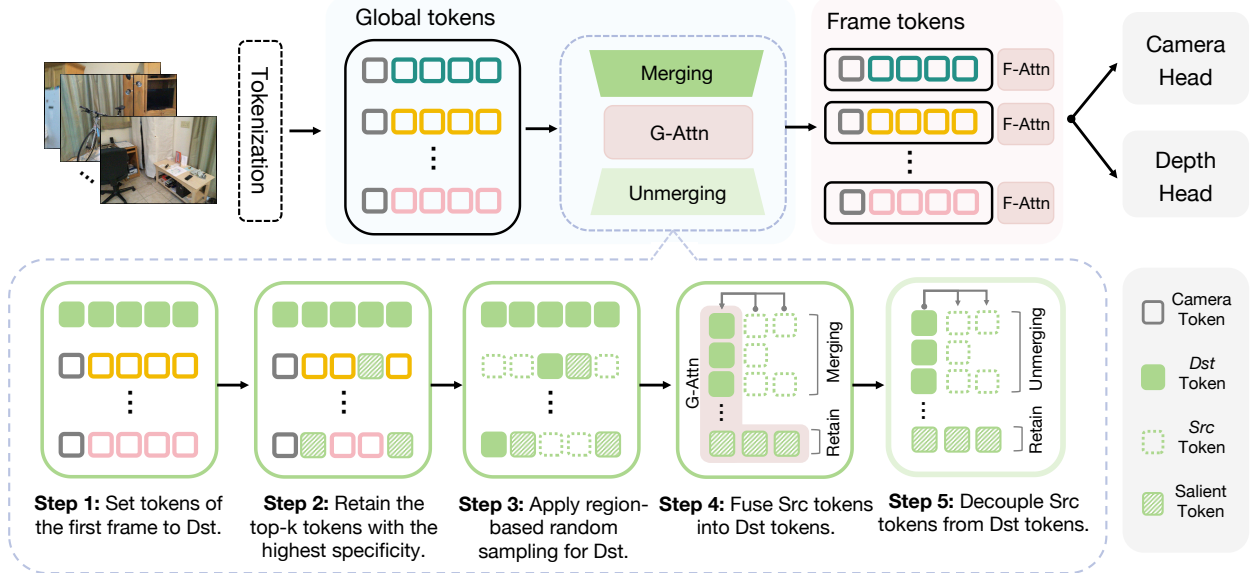


Figure 4. Visualizations of the Global Attention maps in VGGT, using six representative tokens (including the camera token and several image tokens), show that at every stage the attention patterns of different tokens exhibit a strong degree of similarity. G-Attn and F-Attn denote Global Attention and Frame Attention, respectively.

3.2. Token Partitioning

In contrast to token merging methods primarily developed for 2D vision tasks, which typically operate on individual images, feed-forward 3D reconstruction models process multi-view sequences with varying degrees of overlap across viewpoints. Such overlaps are critical for accurate 3D reconstruction, as they provide the cross-view correspondences necessary for recovering consistent geometry. Therefore, to achieve acceleration through merging while preserving reconstruction fidelity, it becomes essential to design an effective token partitioning strategy that operates across all frames in the sequence.

The design of our token partitioning strategy is governed by three principles: 1) preserving cross-frame correspondence to ensure structural consistency of the overall scene; 2) ensuring uniform merging within each frame to prevent both over-compression and redundancy; and 3) merging the most redundant tokens into the most representative ones to maximize acceleration efficiency. Accordingly, we divide tokens into three categories: salient tokens, which capture the most distinctive features of each frame; destination (dst) tokens, which act as representative anchors; and source (src) tokens, which correspond to redundant information to be merged. Based on these principles, we design three token partitioning strategies as detailed in the following.

Reference Token Selection. First, VGGT defines the first frame as the world coordinate system, with all tokens registered relative to this reference. This design makes the first frame a key anchor for maintaining spatial consistency

across the sequence. Supplementary visualization of attention maps further shows that tokens consistently exhibit stronger activations toward the first frame than any other, highlighting its central role in guiding scene-level representations. Consequently, we designate all tokens from the first frame as dst tokens due to their strong representativeness.

Salient Token Selection. Second, since VGGT reconstructs scenes through cross-frame token interactions, a subset of key tokens is critical for establishing reliable correspondences across views. As illustrated in Figure 3, these tokens resemble distinctive keypoints in traditional matching algorithms. To preserve them, we extend conventional token merging by introducing a third category, dividing tokens into salient, dst, and src groups. Salient tokens are excluded from merging operations and instead participate directly in attention. For selecting salient tokens, we first apply a top-k strategy based on token norms to measure distinctiveness. However, its computational overhead grows with longer sequences. To improve efficiency, we adopt a fixed-stride sampling scheme that retains about 10% of tokens per frame as salient tokens, serving as anchors to maintain distinctiveness. Experiments show that this achieves accuracy comparable to top-k selection while greatly reducing cost. We therefore use fixed-stride sampling as the default strategy, balancing efficiency and effectiveness.

Uniform Token Sampling. Finally, recognizing the dense prediction nature of 3D reconstruction, we ensure uniform intra-frame sampling to avoid local over-compression or redundancy. To this end, we assign dst and src tokens within

each frame using a region-based random sampling strategy inspired by the success of ToMeSD [1] in diffusion models. Concretely, we first partition the input tokens by frame and arrange them into a 2D grid of image patches. Within each grid cell, dst tokens are sampled according to a predefined merging ratio with stride K , while the remaining tokens are designated as src tokens. This region-based strategy ensures spatially balanced merging and prevents artifacts such as the disappearance of large areas. Consequently, the merging process is more coherent, and the reconstructed scene better preserves global structural stability.

3.3. Token Merging Procedure

After token partitioning, src tokens are merged into their most similar counterparts in dst, effectively reducing the sequence length for attention computation. Formally, given a token representation $x \in \mathbb{R}^c$ with feature dimension c , we compute cosine similarity between each $x_s \in \text{src}$ and all $x_d \in \text{dst}$:

$$\text{sim}(x_s, x_d) = \frac{x_s \cdot x_d}{\|x_s\| \|x_d\|}. \quad (1)$$

Each source token x_s is assigned to its most similar destination token x_d , and updated by averaging:

$$x'_d = \frac{x_d + x_s}{2}. \quad (2)$$

The updated x'_d is retained while x_s is temporarily discarded, thereby reducing the number of tokens processed in attention computations.

3.4. Token Unmerging Procedure

Dense 3D reconstruction requires per-token outputs (*e.g.*, depth predictions). To satisfy this requirement, we adopt an unmerging operation, inspired by ToMeSD [1], which restores the original token resolution and maintains full compatibility with the VGGT architecture. Specifically, suppose two tokens $x_1, x_2 \in \mathbb{R}^c$ are merged into a single representation:

$$x_{1,2}^* = \frac{x_1 + x_2}{2}. \quad (3)$$

During unmerging, this representation is replicated to recover the original sequence length:

$$x'_1 = x_{1,2}^* \quad x'_2 = x_{1,2}^* \quad (4)$$

This replication guarantees that the token count matches the input resolution, allowing the decoder to produce dense outputs for every patch. Moreover, by maintaining an explicit src–dst mapping during merging, the unmerging process is both deterministic and efficient. This ensures that the model enjoys the computational benefits of a compressed sequence in the Global Attention layers, while still delivering the per-token predictions.

3.5. VRAM-Efficient Implementation

In our tests, the original VGGT encounters out-of-memory errors when processing sequences of around 300 frames. VGGT consists of 24 encoder blocks, but during inference only the outputs of layers 4, 11, 17, and 23 are required. Nevertheless, the original implementation stores intermediate results from all 24 blocks. To support longer input sequences, we introduce an simple optimized variant, VGGT*, which discards unused intermediate outputs during inference. This reduces memory consumption and enables processing of up to 1000 frames without affecting reconstruction quality. Unless otherwise specified, all experiments in this paper use VGGT* as the baseline.

4. Experiments

4.1. Experimental Setup

We evaluate FastVGGT on three benchmark datasets: ScanNet, NRGDB, and 7 Scenes. For ScanNet, which contains 1,500 scenes, we uniformly sample 50 scenes to form a reproducible benchmark, denoted as ScanNet-50. Our experiments focus on two tasks: camera pose estimation and point map reconstruction. Across both tasks, FastVGGT consistently achieves substantial speedups while maintaining accuracy. The overall architecture follows VGGT, comprising L=24 frame and global attention layers, with Flash-Attention2 [6] integrated to further accelerate inference. All experiments are conducted on a workstation with an NVIDIA A800 GPU (80 GiB VRAM).

4.2. 3D Reconstruction

Comparisons on the ScanNet-50 Dataset. We begin by evaluating FastVGGT on the ScanNet-50 dataset, reporting reconstruction quality using Chamfer Distance (CD). Experiments are conducted with input sequences of 1000, 500, and 100 images, enabling us to assess performance under varying sequence lengths. The results in Table 2 show that although SOTA methods such as π^3 and StreamVGGT achieve strong performance on short sequences, they fail on long sequences due to memory constraints. Methods like Fast3R [30] and CUT3R [26] can process long sequences efficiently, but their reconstruction quality degrades severely. In contrast, FastVGGT delivers substantial acceleration over baseline VGGT across all settings while preserving reconstruction accuracy. Notably, when processing very long sequences (*e.g.*, 1000 images), FastVGGT not only maintains reconstruction fidelity but also significantly mitigates error accumulation, demonstrating robustness and scalability for large-scale 3D reconstruction.

Comparisons on 7 Scenes and NRGDB Datasets. Following the CUT3R protocol, we evaluate FastVGGT on the 7 Scenes and NRGDB datasets. We report accuracy

Method	1000		500		300		100	
	CD ↓	Time ↓	CD ↓	Time ↓	CD ↓	Time ↓	CD ↓	Time ↓
π^3 [29]	<i>OOM</i>	<i>OOM</i>	<i>OOM</i>	<i>OOM</i>	<i>OOM</i>	<i>OOM</i>	<i>OOM</i>	<i>OOM</i>
StreamVGGT [33]	<i>OOM</i>	<i>OOM</i>	<i>OOM</i>	<i>OOM</i>	<i>OOM</i>	<i>OOM</i>	<i>OOM</i>	<i>OOM</i>
Fast3R [30]	0.684	397.8s	0.701	97.3s	0.711	34.9s	0.723	4.8s
CUT3R [26]	0.786	34.8s	0.774	18.8s	0.775	11.1s	0.767	3.6s
VGGT* [25]	0.471	724.6s	0.420	177.5s	0.416	131.4s	0.423	9.1s
FastVGGT	0.425	180.7s	0.411	55.2s	0.416	23.8s	0.426	5.4s

Table 2. Quantitative results of point cloud reconstruction on the ScanNet-50 dataset with input sequences of 1000, 500, 300, and 100 images. *OOM* denotes out-of-memory.

Method	7 Scenes - Stride 3							7 Scenes - Stride 10						
	Acc ↓		Comp ↓		NC ↑		Time ↓	Acc ↓		Comp ↓		NC ↑		Time ↓
	Mean	Med.	Mean	Med.	Mean	Med.		Mean	Med.	Mean	Med.	Mean	Med.	
π^3 [29]	<i>OOM</i>	<i>OOM</i>	<i>OOM</i>	<i>OOM</i>	<i>OOM</i>	<i>OOM</i>	<i>OOM</i>	<i>OOM</i>	<i>OOM</i>	<i>OOM</i>	<i>OOM</i>	<i>OOM</i>	<i>OOM</i>	<i>OOM</i>
StreamVGGT [33]	<i>OOM</i>	<i>OOM</i>	<i>OOM</i>	<i>OOM</i>	<i>OOM</i>	<i>OOM</i>	<i>OOM</i>	<i>OOM</i>	<i>OOM</i>	<i>OOM</i>	<i>OOM</i>	<i>OOM</i>	<i>OOM</i>	<i>OOM</i>
Fast3R [30]	0.045	0.027	0.047	0.010	0.616	0.627	43.7s	0.040	0.021	0.056	0.013	0.639	0.657	5.5s
CUT3R [26]	0.179	0.121	0.097	0.043	0.588	0.581	14.5s	0.041	0.021	0.029	0.010	0.651	0.677	4.2s
VGGT* [25]	0.019	0.008	0.027	0.010	0.611	0.628	76.7s	0.020	0.008	0.027	0.010	0.623	0.641	8.7s
FastVGGT	0.018	0.008	0.026	0.010	0.617	0.634	28.0s	0.018	0.008	0.027	0.010	0.628	0.648	5.1s

Table 3. Quantitative results of point cloud reconstruction on the 7 Scenes dataset. Stride denotes keyframes sampled every 3 or 10 frames.

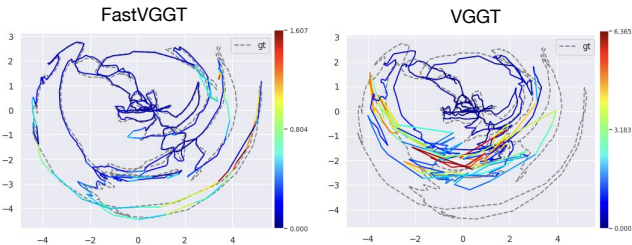


Figure 5. Comparison of pose estimation performance between FastVGGT and VGGT.

(Acc), completeness (Comp), and normal consistency (NC) using long-sequence inputs, with keyframes sampled every 3 or 10 frames. As shown in Table 3 and Table 4, FastVGGT maintains the robust performance demonstrated on ScanNet-50, further demonstrating its effectiveness for 3D reconstruction.

4.3. Camera Pose Estimation

We begin by evaluating FastVGGT on the ScanNet-50 dataset, reporting reconstruction quality with Chamfer Distance (CD). Experiments are conducted with input sequences of 1000, 500, and 100 images, allowing us to assess performance across different sequence lengths. As summarized in Table 2, state-of-the-art methods such as π^3

and StreamVGGT achieve strong results on short sequences but fail on long ones due to memory limitations. Methods like Fast3R [30] and CUT3R [26] can handle longer sequences efficiently, yet their reconstruction quality drops significantly. In contrast, FastVGGT achieves substantial acceleration over baseline VGGT across all settings while preserving reconstruction accuracy. Notably, on very long sequences (e.g., 1000 images), FastVGGT not only maintains reconstruction fidelity but also mitigates error accumulation, demonstrating robustness and scalability for large-scale 3D reconstruction.

We further evaluate FastVGGT on the 7 Scenes and NRGBD datasets following the CUT3R protocol. Performance is measured by accuracy (Acc), completeness (Comp), and normal consistency (NC) using long-sequence inputs, where keyframes are sampled every 3 or 10 frames. Results in Table 3 and Table 4 show that FastVGGT sustains the robust performance observed on ScanNet-50 and achieves competitive or superior results across all metrics. These experiments confirm that FastVGGT generalizes well beyond ScanNet-50, providing consistent improvements in reconstruction quality and efficiency across diverse scenes, thereby underscoring its practicality for real-world 3D vision applications.

Method	NRGBD - Stride 3								NRGBD - Stride 10							
	Acc ↓		Comp ↓		NC ↑		Time ↓	Acc ↓		Comp ↓		NC ↑		Time ↓		
	Mean	Med.	Mean	Med.	Mean	Med.		Mean	Med.	Mean	Med.	Mean	Med.			
π^3 [29]	<i>OOM</i>	<i>OOM</i>	<i>OOM</i>	<i>OOM</i>	<i>OOM</i>	<i>OOM</i>	<i>OOM</i>	<i>OOM</i>	<i>OOM</i>	<i>OOM</i>	<i>OOM</i>	<i>OOM</i>	<i>OOM</i>	<i>OOM</i>	<i>OOM</i>	
StreamVGGT [33]	<i>OOM</i>	<i>OOM</i>	<i>OOM</i>	<i>OOM</i>	<i>OOM</i>	<i>OOM</i>	<i>OOM</i>	<i>OOM</i>	<i>OOM</i>	<i>OOM</i>	<i>OOM</i>	<i>OOM</i>	<i>OOM</i>	<i>OOM</i>	<i>OOM</i>	
Fast3R [30]	0.074	0.036	0.024	0.011	0.658	0.682	68.9s	0.061	0.028	0.031	0.013	0.669	0.712	7.4s		
CUT3R [26]	0.346	0.243	0.184	0.090	0.579	0.623	18.3s	0.132	0.064	0.056	0.0106	0.669	0.725	5.7s		
VG GT* [25]	0.029	0.019	0.018	0.009	0.727	0.728	136.1s	0.016	0.010	0.017	0.009	0.735	0.738	13.9s		
FastVG GT	0.029	0.021	0.019	0.010	0.730	0.738	53.1s	0.018	0.011	0.018	0.009	0.736	0.741	7.3s		

Table 4. Quantitative results of point cloud reconstruction on the NRGBD dataset.

Input	ATE ↓		ARE ↓		RPE-rot ↓		RPE-trans ↓	
	Frames	Baseline	Ours	Baseline	Ours	Baseline	Ours	Baseline
1000	0.196	0.164	4.636	3.860	0.997	0.667	0.039	0.029
500	0.174	0.145	4.190	3.591	0.963	0.627	0.042	0.031
300	0.145	0.142	3.689	3.554	0.786	0.801	0.040	0.036
100	0.140	0.141	3.625	3.512	1.224	1.262	0.058	0.061

Table 5. Quantitative results of camera pose estimation on the ScanNet-50 dataset.

Methods	Uniform	Reference	Salient	CD ↓	ATE ↓
(a)	-	-	-	0.947	0.842
(b)	✓	-	-	0.637	0.722
(c)	✓	✓	-	0.431	0.149
(d)	✓	✓	✓	0.411	0.141

Table 6. Ablation study for Token partitioning strategies.

Blocks	0.3		0.6		0.9	
	CD ↓	Time ↓	CD ↓	Time ↓	CD ↓	Time ↓
0	0.408	119.8s	0.415	64.3s	0.411	55.2s
10	0.418	146.2s	0.424	118.4s	0.431	106.3s
20	0.423	172.9s	0.427	169.1s	0.411	157.3s

Table 7. Ablation study on merging ratio and affected blocks.

4.4. Ablation Studies

Token Partitioning. We evaluate the effectiveness of different token partitioning strategies using 500-frame inputs from ScanNet-50. As shown in Table 6: (a) directly selecting dst and src tokens through random sampling yields poor performance; (b) adopting region-based intra-frame uniform sampling improves performance but remains sub-optimal; (c) designating the global reference frame (first frame) as dst tokens brings substantial gains; and (d) further protecting salient tokens leads to the best performance.

Location and Intensity of Merging. To balance accuracy and efficiency, we evaluate the effect of varying the starting block for merging and the applied merging ratio. As shown in Table 7, increasing the merging ratio consistently reduces inference time, with only minor fluctuations in Chamfer Distance. Consequently, we adopt an aggressive strategy that applies a 90% merging ratio from block 0 across all subsequent layers, yielding a favorable balance of accuracy and efficiency.

5. Conclusion

In this work, we proposed Fast-VGGT, a training-free method that accelerates VGGT inference via strategic token merging without sacrificing reconstruction quality. By profiling VGGT, we identified the global attention module as the primary bottleneck for long-sequence inputs and observed strong similarities in its attention maps. To address this, we introduce token merging to alleviate the inference bottleneck and design strategies tailored to the feed-forward visual geometry model. Experiments on multiple benchmarks show that FastVG GT achieves up to 4x speedup on 1000-images inputs while maintaining competitive accuracy in both camera pose estimation and 3D reconstruction tasks, and further mitigates error accumulation in long-sequence settings. These results highlight token merging as a principled solution for scaling visual geometry models and demonstrate FastVG GT’s immediate practicality for real-world applications.

References

- [1] Daniel Bolya and Judy Hoffman. Token merging for fast stable diffusion. In *Proceedings of the IEEE/CVF conference on computer vision and pattern recognition*, pages 4599–4603, 2023. [2](#), [6](#)
- [2] Daniel Bolya, Cheng-Yang Fu, Xiaoliang Dai, Peizhao Zhang, Christoph Feichtenhofer, and Judy Hoffman. Token merging: Your vit but faster. *arXiv preprint arXiv:2210.09461*, 2022. [2](#), [3](#)
- [3] Qingqing Cao, Bhargavi Paranjape, and Hannaneh Hajishirzi. Pumer: Pruning and merging tokens for efficient vision language models. *arXiv preprint arXiv:2305.17530*, 2023. [3](#)
- [4] Mathilde Caron, Hugo Touvron, Ishan Misra, Hervé Jégou, Julien Mairal, Piotr Bojanowski, and Armand Joulin. Emerging properties in self-supervised vision transformers. In *Proceedings of the IEEE/CVF international conference on computer vision*, pages 9650–9660, 2021. [3](#)
- [5] Joonmyung Choi, Sanghyeok Lee, Jaewon Chu, Minhyuk Choi, and Hyunwoo J Kim. vid-tldr: Training free token merging for light-weight video transformer. In *Proceedings of the IEEE/CVF Conference on Computer Vision and Pattern Recognition*, pages 18771–18781, 2024. [3](#)
- [6] Tri Dao. Flashattention-2: Faster attention with better parallelism and work partitioning. *arXiv preprint arXiv:2307.08691*, 2023. [6](#)
- [7] Kai Deng, Zexin Ti, Jiawei Xu, Jian Yang, and Jin Xie. Vggt-long: Chunk it, loop it, align it–pushing vggt’s limits on kilometer-scale long rgb sequences. *arXiv preprint arXiv:2507.16443*, 2025. [3](#)
- [8] Alexey Dosovitskiy, Lucas Beyer, Alexander Kolesnikov, Dirk Weissenborn, Xiaohua Zhai, Thomas Unterthiner, Mostafa Dehghani, Matthias Minderer, Georg Heigold, Sylvain Gelly, et al. An image is worth 16x16 words: Transformers for image recognition at scale. *arXiv preprint arXiv:2010.11929*, 2020. [3](#)
- [9] Joakim Bruslund Haurum, Sergio Escalera, Graham W Taylor, and Thomas B Moeslund. Which tokens to use? investigating token reduction in vision transformers. In *Proceedings of the IEEE/CVF International Conference on Computer Vision*, pages 773–783, 2023. [3](#)
- [10] Seon-Ho Lee, Jue Wang, Zhikang Zhang, David Fan, and Xinyu Li. Video token merging for long-form video understanding. *arXiv preprint arXiv:2410.23782*, 2024. [2](#)
- [11] Vincent Leroy, Yohann Cabon, and Jérôme Revaud. Grounding image matching in 3d with mast3r. In *European Conference on Computer Vision*, pages 71–91. Springer, 2024. [2](#), [3](#)
- [12] Raul Mur-Artal and Juan D Tardós. Orb-slam2: An open-source slam system for monocular, stereo, and rgbd cameras. *IEEE transactions on robotics*, 33(5):1255–1262, 2017. [3](#)
- [13] Raul Mur-Artal, Jose Maria Martinez Montiel, and Juan D Tardos. Orb-slam: A versatile and accurate monocular slam system. *IEEE transactions on robotics*, 31(5):1147–1163, 2015. [3](#)
- [14] Maxime Oquab, Timothée Darcet, Théo Moutakanni, Huy Vo, Marc Szafraniec, Vasil Khalidov, Pierre Fernandez, Daniel Haziza, Francisco Massa, Alaeldin El-Nouby, et al. Dinov2: Learning robust visual features without supervision. *arXiv preprint arXiv:2304.07193*, 2023. [3](#)
- [15] Yansong Qu, Yuze Wang, and Yue Qi. Sg-nerf: Semantic-guided point-based neural radiance fields. In *2023 IEEE International Conference on Multimedia and Expo (ICME)*, pages 570–575. IEEE, 2023. [2](#)
- [16] Yansong Qu, Shaohui Dai, Xinyang Li, Yuze Wang, You Shen, Liujuan Cao, and Rongrong Ji. Deocc-1-to-3: 3d deocclusion from a single image via self-supervised multi-view diffusion. *arXiv preprint arXiv:2506.21544*, 2025. [2](#)
- [17] Cedric Renggli, André Susano Pinto, Neil Houlsby, Basil Mustafa, Joan Puigcerver, and Carlos Riquelme. Learning to merge tokens in vision transformers. *arXiv preprint arXiv:2202.12015*, 2022. [3](#)
- [18] Michael Ryoo, AJ Piergiovanni, Anurag Arnab, Mostafa Dehghani, and Anelia Angelova. Tokenlearner: Adaptive space-time tokenization for videos. *Advances in neural information processing systems*, 34:12786–12797, 2021. [3](#)
- [19] Johannes L Schonberger and Jan-Michael Frahm. Structure-from-motion revisited. In *Proceedings of the IEEE conference on computer vision and pattern recognition*, pages 4104–4113, 2016. [3](#)
- [20] Leqi Shen, Tianxiang Hao, Tao He, Sicheng Zhao, Yifeng Zhang, Pengzhang Liu, Yongjun Bao, and Guiguang Ding. Tempme: Video temporal token merging for efficient text-video retrieval. *arXiv preprint arXiv:2409.01156*, 2024. [3](#)
- [21] You Shen, Zhipeng Zhang, Xinyang Li, Yansong Qu, Yu Lin, Shengchuan Zhang, and Liujuan Cao. Evolving high-quality rendering and reconstruction in a unified framework with contribution-adaptive regularization. In *Proceedings of the Computer Vision and Pattern Recognition Conference*, pages 16346–16355, 2025. [3](#)
- [22] Oriane Siméoni, Huy V Vo, Maximilian Seitzer, Federico Baldassarre, Maxime Oquab, Cijo Jose, Vasil Khalidov, Marc Szafraniec, Seungeun Yi, Michaël Ramamonjisoa, et al. Dinov3. *arXiv preprint arXiv:2508.10104*, 2025. [3](#), [4](#)
- [23] Zhenggang Tang, Yuchen Fan, Dilin Wang, Hongyu Xu, Rakesh Ranjan, Alexander Schwing, and Zhicheng Yan. Mv-dust3r+: Single-stage scene reconstruction from sparse views in 2 seconds. In *Proceedings of the Computer Vision and Pattern Recognition Conference*, pages 5283–5293, 2025. [2](#)
- [24] Chau Tran, Duy MH Nguyen, Manh-Duy Nguyen, Trung Tin Nguyen, Ngan Le, Pengtao Xie, Daniel Sonntag, James Y Zou, Binh Nguyen, and Mathias Niepert. Accelerating transformers with spectrum-preserving token merging. *Advances in Neural Information Processing Systems*, 37:30772–30810, 2024. [2](#)
- [25] Jianyuan Wang, Minghao Chen, Nikita Karaev, Andrea Vedaldi, Christian Rupprecht, and David Novotny. Vggt: Visual geometry grounded transformer. In *Proceedings of the Computer Vision and Pattern Recognition Conference*, pages 5294–5306, 2025. [2](#), [3](#), [7](#), [8](#)

- [26] Qianqian Wang, Yifei Zhang, Aleksander Holynski, Alexei A Efros, and Angjoo Kanazawa. Continuous 3d perception model with persistent state. In *Proceedings of the Computer Vision and Pattern Recognition Conference*, pages 10510–10522, 2025. [6](#), [7](#), [8](#)
- [27] Shuzhe Wang, Vincent Leroy, Yohann Cabon, Boris Chidlovskii, and Jerome Revaud. Dust3r: Geometric 3d vision made easy. In *Proceedings of the IEEE/CVF Conference on Computer Vision and Pattern Recognition*, pages 20697–20709, 2024. [2](#), [3](#)
- [28] Yuze Wang, Junyi Wang, Ruicheng Gao, Yansong Qu, Wantong Duan, Shuo Yang, and Yue Qi. Look at the sky: Sky-aware efficient 3d gaussian splatting in the wild. *IEEE Transactions on Visualization and Computer Graphics*, 2025. [3](#)
- [29] Yifan Wang, Jianjun Zhou, Haoyi Zhu, Wenzheng Chang, Yang Zhou, Zizun Li, Junyi Chen, Jiangmiao Pang, Chunhua Shen, and Tong He. Scalable permutation-equivariant visual geometry learning. *arXiv preprint arXiv:2507.13347*, 2025. [7](#), [8](#)
- [30] Jianing Yang, Alexander Sax, Kevin J Liang, Mikael Henaff, Hao Tang, Ang Cao, Joyce Chai, Franziska Meier, and Matt Feiszli. Fast3r: Towards 3d reconstruction of 1000+ images in one forward pass. In *Proceedings of the Computer Vision and Pattern Recognition Conference*, pages 21924–21935, 2025. [2](#), [6](#), [7](#), [8](#)
- [31] Wang Zeng, Sheng Jin, Wentao Liu, Chen Qian, Ping Luo, Wanli Ouyang, and Xiaogang Wang. Not all tokens are equal: Human-centric visual analysis via token clustering transformer. In *Proceedings of the IEEE/CVF conference on computer vision and pattern recognition*, pages 11101–11111, 2022. [3](#)
- [32] Shangzhan Zhang, Jianyuan Wang, Yinghao Xu, Nan Xue, Christian Rupprecht, Xiaowei Zhou, Yujun Shen, and Gordon Wetzstein. Flare: Feed-forward geometry, appearance and camera estimation from uncalibrated sparse views. In *Proceedings of the Computer Vision and Pattern Recognition Conference*, pages 21936–21947, 2025. [2](#)
- [33] Dong Zhuo, Wenzhao Zheng, Jiahe Guo, Yuqi Wu, Jie Zhou, and Jiwen Lu. Streaming 4d visual geometry transformer. *arXiv preprint arXiv:2507.11539*, 2025. [7](#), [8](#)